

## An Electron Diffraction Investigation of the Structures of Neopentyl Chloride and SilicoNeopentyl Chloride: The Determination of Intensities through the Use of a Rotating Sector

J. M. Hastings and S. H. Bauer

Citation: [The Journal of Chemical Physics](#) **18**, 13 (1950); doi: 10.1063/1.1747431

View online: <http://dx.doi.org/10.1063/1.1747431>

View Table of Contents: <http://scitation.aip.org/content/aip/journal/jcp/18/1?ver=pdfcov>

Published by the [AIP Publishing](#)

---

### Articles you may be interested in

[Accurate growth rate determination on rotating substrates using electron diffraction dynamics](#)

Appl. Phys. Lett. **74**, 138 (1999); 10.1063/1.122975

[Electron diffraction investigation of the molecular structure and amplitudes of vibration of gaseous thiazyl chloride, NSCl](#)

J. Chem. Phys. **58**, 2195 (1973); 10.1063/1.1679491

[On the Mechanism of the Pyrolysis of Neopentyl Chloride](#)

J. Chem. Phys. **39**, 1673 (1963); 10.1063/1.1734512

[The Use of Punched Cards in Molecular Structure Determinations II. Electron Diffraction Calculations](#)

J. Chem. Phys. **14**, 659 (1946); 10.1063/1.1724082

[The Electron Diffraction Investigation of the Molecular Structures of Ketene and Thiophosphoryl Chloride](#)

J. Chem. Phys. **6**, 75 (1938); 10.1063/1.1750206

---



# An Electron Diffraction Investigation of the Structures of Neopentyl Chloride and Silico-Neopentyl Chloride

## The Determination of Intensities through the Use of a Rotating Sector

J. M. HASTINGS\* AND S. H. BAUER

Department of Chemistry, Cornell University, Ithaca, New York

(Received April 25, 1949)

Constructional details and operational data on an electron diffraction apparatus, in which a rotating sector has been incorporated, are presented. Its range of application and limitations are listed, and methods for the reduction of microphotometer records are discussed.

Electron diffraction photographs of neopentyl chloride and silico-neopentyl chloride were taken with and without sectors. Their structures were deduced by a combination of the visual and photometric procedures. Attempts were made to estimate quantitatively the equivalent temperature factors for libration about the C—C and Si—C bonds. Best values for the interatomic distances and their possible interpretations are presented in the concluding section.

IN this and in the two papers which follow we shall present structural conclusions based on electron diffraction patterns of gases obtained with and without the use of a rotating sector. An abbreviated description of the apparatus will be given, since the essential conclusions regarding the structures of the compounds discussed do not depend on the sector data. On the other hand, the description will be adequate enough to permit an assessment of the validity of those conclusions which do depend on the sector data. The apparatus utilized in these studies has since been improved; an analysis of the fundamentals and limitations of the sector technic, and of the design features which have been incorporated to reduce some of these limitations, will be published in another journal.<sup>†</sup>

### FUNDAMENTAL EQUATIONS

The ratio of the intensity scattered at an angle  $\theta$  to the power in the primary beam is given by<sup>1</sup>

$$\frac{I(s)}{P_0} = \left[ \frac{8\pi^2 m e^2}{h^2} \right]^2 \frac{N}{R^2 s^4} \left\{ \sum_i f_i^2 + \sum_i G_i + \sum_i' \sum_j' f_i f_j \right. \\ \left. \times \int_0^\infty P(r_{ij}) \frac{\sin s r_{ij}}{s r_{ij}} dr_{ij} \right\}, \quad (1)$$

where  $N$  = number of scattering units per unit area of beam;  $R$  = distance from scattering point to detector;  $s = (4\pi/\lambda) \sin \theta / 2$ ;  $f_i$ ,  $G_i$  = coherent, incoherent atom form factors;  $f_i = (Z_i - F_i)$ ;  $F_i$  = x-ray atom form factor, coherent;  $r_{ij}$  = distance between atoms  $i$  and  $j$  in the scattering unit;  $P(r_{ij})$  = probability distribution in  $r_{ij}$  due to interatomic motions within each scattering unit.

The other symbols have their usual meanings. The observable range of  $s$  extends from about 1.5 to a maximum of 35 for most cameras, while the variation in intensity over this range is roughly  $10^4$  to 1, due to the  $1/s^4$  factor. Since photographic materials are approximately linear over a range of 100/1, photographic recording of electron intensity permits an objective quantitative evaluation of only a small interval of the intensity at any one time. Furthermore, the steep declining slope on which the oscillating term is superposed transforms the maxima and minima to inflections or derivatives of higher order. In Fig. 1 the electron current which might be received by a collector is plotted as a function of  $s$  for hexamethylcyclotrisiloxane.

To obtain a photographic record of  $I(s)/P_0$ , which can be treated quantitatively over the entire range of  $s$ , one must multiply the pattern, prior to recording, by a function which will reduce the range of electron intensity. Then the maxima and minima of the third term appear as such rather than as inflections. A number of investigators<sup>2</sup> have accomplished this through the use of a sector—a heart-shaped mask which rotates about an axis which lies along the undeflected ray, in a plane in front of and parallel to the photographic plate; the sector in effect, limits the time of exposure as some function of  $s$  (see Fig. 2).

The accuracy of the determination of interatomic distances is limited not only by the precision of the evaluation of  $I(s)/P_0$ , but also by the relative magnitude of the molecular to the atomic terms in the scattering equation. Even if the background term is reduced to unity with an appropriate sector, this limitation is a severe one since the ratio of molecular to atomic contributions

\* Present address: Brookhaven National Laboratory, Upton, New York.

<sup>†</sup> A major portion of this analysis has been presented in a report to ONR by Bauer, Keidel, and Harvey, February 1949, submitted under Contract No. N6 ori-213, Task Order I.

<sup>1</sup> P. J. W. Debye, J. Chem. Phys. 9, 55 (1941).

<sup>2</sup> (a) F. Trendelenburg, Naturwiss. 21, 175 (1933); Physik. Zeits. 40, 727 (1939). (b) P. Debye, Physik. Zeits. 40, 404 (1939). (c) Finbak, Hassel, and Ottar, Arch. Math. Naturv. B44, No. 13 (1941). (d) H. J. Yearian, Phys. Rev. 59, 926 (1941). (e) S. H. Bauer, Phys. Rev. 64, 316 (1943). (f) H. Viervoll, Acta Chem. Scand. 1, 120 (1947). (g) H. J. Yearian and W. M. Barss, J. App. Phys. 19, 700 (1948).

declines as  $\exp(-a^2s^2)/s$ , with typical values for  $a^2$  around 0.002. For the case of hexamethylcyclotrisiloxane, if  $I(s)/P_0$  were determined to one percent (densitometry rarely leads to values so reliable), then it would be possible to estimate the molecular term to an accuracy of approximately three percent at  $s=5$ ; seven percent at  $s=10$ ; 30 percent at  $s=20$ ; and 100 percent at  $s=30$ . To increase the precision of these determinations one must either increase the precision of evaluation of  $I(s)/P_0$ , or subtract from the pattern, prior to recording, a major portion of the atomic contribution. The impossibility of performing this subtraction is inherent in photographic recording. Whether it could be successfully done by direct measurement of the diffraction current is being investigated in this laboratory.

To reduce the background term to unity, the fractional opening of the sector should be

$$[\phi/\pi] = \frac{s^4}{\sum_i f_i^2 + \sum_i G_i} \quad (2)$$

then,

$$\left[\frac{I(s)}{P_0}\right]_{\text{sector}} = \left[\frac{8\pi^2 mc^2}{h^2}\right]^2 \frac{N}{R^2} \left\{ 1 + \frac{\sum' \sum' f_i f_j}{\sum f_i^2 + \sum G_i} \times \int_0^\infty P(r_{ij}) \frac{\sin sr_{ij}}{sr_{ij}} dr_{ij} \right\}. \quad (3)$$

Equations (1) and (3) are idealized relations, for in their derivation one assumed, besides absolute monochromaticity, that the electron beam may be represented by a plane parallel wave of infinitesimal width both at the sector and at the plate; further, that the sample of  $N$  molecules extends over a region negligibly small compared to the dimensions of  $R$ ; finally, that no multiple scattering occurs. In practice none of these is satisfied in the usual experimental arrangements. The beam has finite width at the plate—0.01 to 0.04 cm; the sample diffuses out of the nozzle into the camera section; multiple scattering may remove up to five percent of the primary diffracted rays, if nozzle pressures are as high as

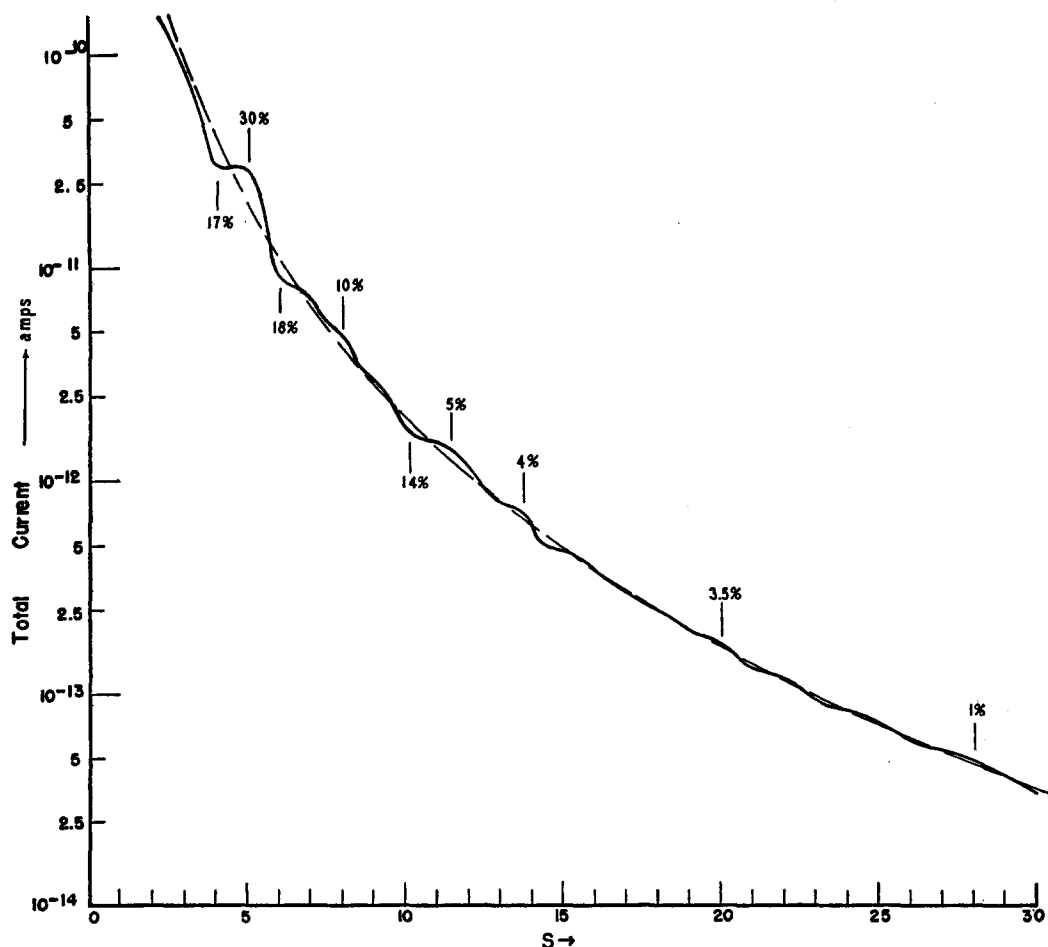


FIG. 1. Collector current expected for electrons diffracted by  $[(\text{CH}_3)_2\text{SiO}]_3$  vapor, under the following conditions:  $N=4.09 \times 10^{14}$ ;  $R=20$  cm; collector  $0.01 \times 0.20$  cm (narrow dimension equivalent  $\Delta s=0.057$  unit);  $P_0=1 \times 10^{-6}$  amp.

three mm Hg. For visual work the loss in resolution introduced by these effects is of no particular consequence except in the estimation of temperature factors. For sector work, however, the fact that the experimental arrangement does not satisfy the conditions implied by the equation must be considered.<sup>3</sup> We have made extensive computations to determine the magnitude of loss in resolution arising from finite extension of the sample, multiple scattering and imperfect focusing of the primary ray; these can be allowed for in the interpretation of the reduced microphotometer records.

### THE APPARATUS

In Fig. 3, top and side views of the electron diffraction unit are shown. Items 1, 2, and 3 are the electron gun, biasing cup, and anode, respectively. A set of collimating holes, 0.010 in., 0.050 in., and 0.062 in. follows; 4 is a set of vertical and horizontal deflecting plates across which a controlled potential of 50–150 volts is placed in order to permit the accurate location of the electron beam at the center of rotation of the sector. The horizontal set also serves as a shutter when 2000 volts are impressed across it. Item 5 is a magnetic lens, while 6a, 6b are top and side views, respectively, of a high temperature nozzle. This design permits the interposing of calibrating samples (gold foil, zinc oxide) at the exact position of the slot through which the gas enters. The region through which the gas passes is heated by conduction; unfortunately, due to thermal leaks in the vicinity of the position control, the section around the bellows valve must be kept 5–10°C higher than the temperature of the nozzle itself.

The sample holder is sketched in Fig. 4. The material either may be placed or distilled into the container, which is then evacuated, and sealed off. After connecting it to the electron diffraction unit by means of the compression coupling, the bellows valve is opened for a short interval, and the thin glass partition is broken by actuating a small external coil. Another type of nozzle useful for room temperature studies is shown in Fig. 5. In both nozzles, provision is made for interposing a platinum stop, several thousandths of an inch wider than

<sup>3</sup> To reduce the magnitude of the extraneous contribution arising from the scattering of the primary beam by the escaped gas and by the residual gas in the camera, a stop was introduced to remove the beam about one cm after the point of maximum gas density. However, this stop also casts a shadow which must be considered in computing the sector shape, as also must be the effect of finite beam size at the sector and extraneous slit and multiple scattering. Consequently, we have replaced (2) by a rather complicated function which formally may be written

$$\left[\frac{\phi}{\pi}\right]_{\text{corr}} = \frac{s^4}{\sum f_i^2 + \sum G_i} \cdot \frac{1}{\text{shadow function}} \cdot \frac{\text{infinitesimal}}{\text{finite beam}} \cdot \left[\frac{\text{extraneous}}{\text{scattering}}\right]. \quad (3a)$$

Since these computations involve averaging processes, we found it more convenient to compute the scattering intensity distribution to be expected under our operating conditions, assuming an approximate sector opening; then we correct the assumed transmission coefficient ( $\phi/\pi$ ) so that a flat background results.

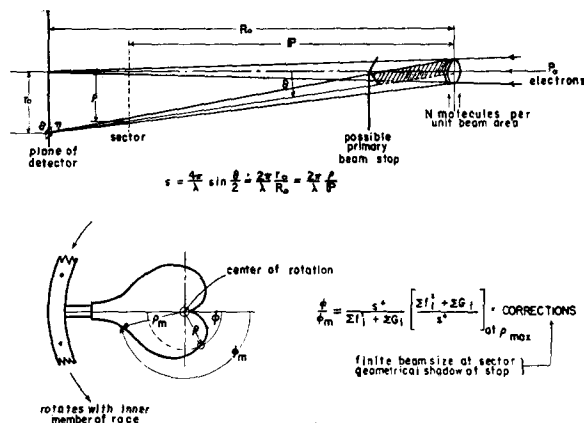


FIG. 2.

the diameter of the primary beam, to remove this beam about 1 cm after the point of maximum gas density.<sup>4</sup>

Returning to Fig. 3, 7 is a gate valve which permits shutting off the main body of the apparatus from the camera section by raising a flap (not shown), actuated through the ground joint, 7a. Thus air may be admitted to the camera, plates changed, and the section pre-pumped through 12, without cooling down the diffusion pumps. Item 8 is the sector assembly; it consists of a precision race the inner member of which carries the heart-shaped mask (8a), several friction drives, and a Wilson seal<sup>5</sup> through which the rotational motion is introduced into the vacuum. The driving motor is located about three feet from the beam to reduce the effects of stray magnetic fields. Directly behind the sector is another platinum cup (9) on an insulated mount. It is not only useful for setting the beam current so that reproducible exposures may be made, but is essential for the positioning of the front beam stop. The latter is adjusted so that on the most sensitive range, the Vance-type electrometer reading is at a minimum. Item 10 is a hexagonal drum which carries one fluorescent and five photographic plates (spectroscopic VD or microfilm for sector work; Eastman Commercial or Panatomic X for visual work). The fluorescent pattern may be observed through the window by means of the front surface mirror, 10a. The drum is rotated by means of gears attached to the flat ground joint, 10b. Various lengths of tubing may be inserted at 11 to allow extension of the sample-plate distance to about 48 cm.

The recent modifications which will be described in a forthcoming paper were made in the construction of the nozzle (6, 6a) sector and camera (8–12) sections.

The accelerating voltage is electronically controlled;<sup>6</sup>

<sup>4</sup> Since the positioning of this stop is extremely critical, a vertical v-shaped strip, the position of which is controlled by a micrometer operating on a 3/1 lever arm is used on the high temperature nozzle (Fig. 3). The first such stop which we introduced (Fig. 5) was circular and hence had to be accurately positioned both vertically and horizontally. It was controlled through a bellows attachment by means of fine thread screws, as shown in the latter figure.

<sup>5</sup> R. R. Wilson, Rev. Sci. Inst. 12, 91 (1941).

<sup>6</sup> Bauer, Hastings, and MacMillan, Rev. Sci. Inst. 14, 30 (1943).



it may be set at any desired value up to about 55 kv and measured to a precision of several hundredths of a percent by a Type K potentiometer spanning a calibrated potential divider. The beam is space-charge limited.<sup>7</sup> Its current (0.1–25  $\mu$ a) is determined in a gross manner by the distance of the filament tip from the hole in the self-biased cup; it may be finely controlled by the magnitude of the biasing resistor. Exposures are pre-set by selecting one of a number of resistors across which a capacitor is discharged; when the potential drops to a given point a thyratron fires and switches on 2000 v across the first set of deflecting plates. Periods ranging from 0.07 to 30 sec. are available. For reference, the controlling circuits are given in Fig. 6. The focused spot is observed by means of a long focal length microscope (20 $\times$  linear magnifications); gold leaf spread on uranium glass affords a low intensity, no-grain screen.

A good vacuum is maintained by two diffusion pumps ( $3\frac{1}{2}$  in. diameter) and three liquid-air traps. Low pressures may be measured by McLeod and ion gauges, while for higher pressures and leak hunting a Pyram gauge was connected to the line at the fore-vacuum end of the diffusion pumps. Between the latter and a Hypervac 20, a baffled liquid-air trap was inserted. This not only keeps the mechanical-pump oil from becoming contaminated by the substances studied, but also allows an increase of about a factor of ten in the sensitivity of the Pyram gauge measurements due to the elimination of the mechanical-pump oil vapors from the vacuum system.

#### OPERATIONAL DATA

Regarding the construction of the sector, we need only indicate that the function (3a) (see reference 3) is transferred onto 0.012 in. aluminum foil<sup>8</sup> by means of an indexing head on a milling machine ( $\phi$  vs.  $\rho$ ), and the two halves of the heart-shaped figure cut and filed simultaneously to a precision of better than 0.001 in. The last operation is performed under a microscope, linear magnification approximately 50. Since the fractional error for each atom species arising from our incomplete knowledge of the atomic scattering functions is

$$\frac{d\phi}{\phi} = n_i \frac{2F_i(Z-F)_i}{\sum (Z-F)_i^2 + \sum G_i F_i} \frac{dF_i}{F_i}, \quad (4)$$

it is the region of small  $\phi$  which is most sensitive, Fig. 7. However, the accuracy in that region is also limited by the extraneous slit and multiple scattering, and by the small net opening in the sector. To reduce the magnitude of the latter, it has been customary to use two sectors, covering the ranges  $0.5 < s < 8$ ;  $0.5 < s < 20$ . (In many cases, the use of a beam stop close to the nozzle exit

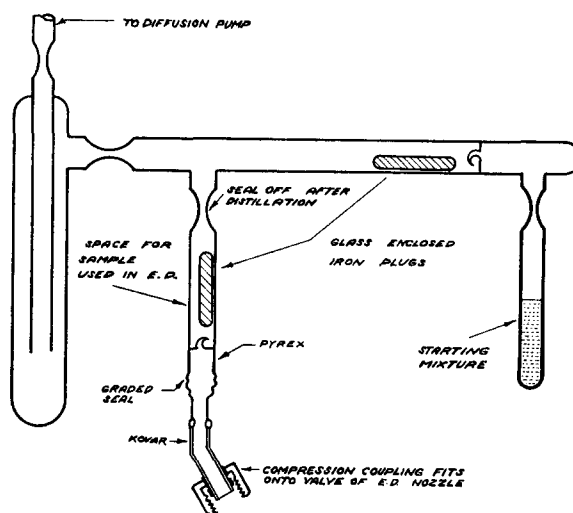


FIG. 4. Sample holder; illustrates manner of handling materials of low volatility without allowing contact with atmosphere of stopcock grease.

eliminates the need for the 0.5–8 sector.) After filing, the sector is mounted and carefully centered so that its geometrical center is within 0.0015 in. of its center of rotation.

Since Eq. (2) implies that a new sector is to be cut for every compound, it is of interest to consider the conditions under which a single sector will serve for a variety of compounds. Inspection of families of reduced atom form factor curves  $[(Z-F)/Z]_i$  suggests that a single sector might be satisfactory for all molecules which consist predominantly of elements within one row of the periodic table. The use of quadratic or cubic sectors has also been proposed. Figures 8(a) and 8(b) are curves showing the backgrounds which would result were the sector openings made proportional to  $s^2$  and  $s^3$ , respectively, for a variety of compounds. If the useful range of photographic density is 0.05 to 1.5,  $s^2$  or  $s^3$  sectors will bring most of the pattern within this density range. However, it is clear that the "drawing-in" of a background is a highly subjective operation under such conditions.

Typical conditions for gas diffraction photography are:

beam current	0.1–2.5 $\mu$ a	film	microfile
exposure time	0.2–0.5 sec.	number of exposures	3–6
reservoir pressure	10–50 mm Hg	1-min. interval between spurts	

sector revolves at approximately 1200 r.p.m.

We have calibrated both microfile and spectroscopic VD plates by running a series of unfocused spot exposures for varying intervals, and found that over the range 0.05–1.00 the density is directly proportional to the intensity.

After aligning the beam with the center of the sector, the current is set at the desired level, the front beam stop interposed and the exposures made. The beam position is then checked, for if it had moved during the exposures

<sup>7</sup> S. G. Ellis, J. App. Phys. 18, 879 (1947) and references cited therein.

<sup>8</sup> Sheet brass or foil of higher atomic number might be preferable; extraneous scattering by edges might thus be reduced.

to the extent of several thousandths of an inch, an incorrect sector function will have been used, particularly for low values of  $s$ .<sup>9</sup>

Unretouched microphotometer recordings of electron diffraction photographs of carbon tetrachloride taken under various conditions are reproduced in Fig. 9, while in Fig. 10 the usefulness of the sector in the study of crystallite size in surface layers<sup>10</sup> is demonstrated.

We have now reached the final point, which relates to the manner of reducing the microphotometer data to intensity values. Two objective procedures have been

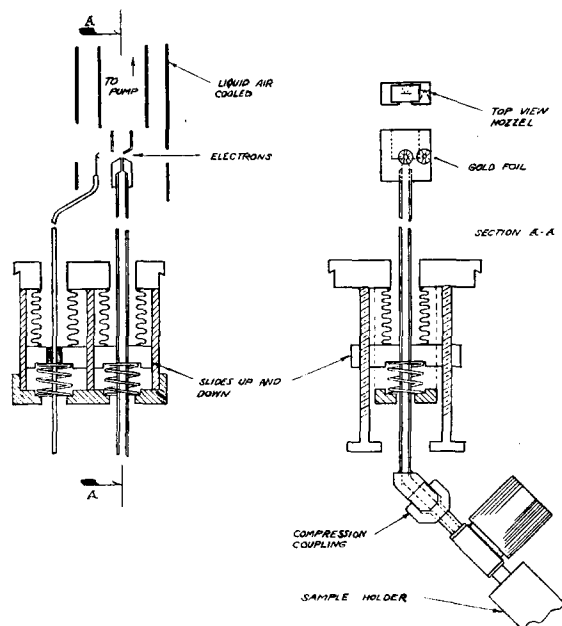


FIG. 5. Room temperature nozzle, with insulated round beam trap.

utilized in drawing in the background, which on the basis of Eq. (3) may be assigned the value unity. Both depend on the availability of theoretical intensity curves (i.e., of the molecular part) for models which are not far from the correct structure.

(A) Average values are computed for the ratios of intensities of adjacent maxima to minima from several theoretical curves. Points are then selected on the microphotometer record for which, if the background were drawn through them, the corresponding ratios for

<sup>9</sup> Slight changes in beam position may be due to fluctuations in the effective electrostatic potential on the deflecting plates due to adsorbed oil films; see A. E. Shaw, *Phys. Rev.* 44, 1006 (1933). The beam position may also be affected by slight motions of the filament due to mechanical vibrations.

<sup>10</sup> In this connection, we should specify that the resolution obtainable with our instrument is  $1/83$ , an average value of that measured for the (220), (311), (331), and (420) rings of gold. The definition of resolution is the one given by J. Hillier and R. F. Baker, *J. App. Phys.* 17, 12 (1946):

$$\left(\frac{\Delta d}{d}\right)_{hkl} = \frac{1.73w}{2} \frac{d_{hkl}}{R}, \quad (4a)$$

wherein  $w$  is the observed width at half-maximum of the trace for the corresponding ring.

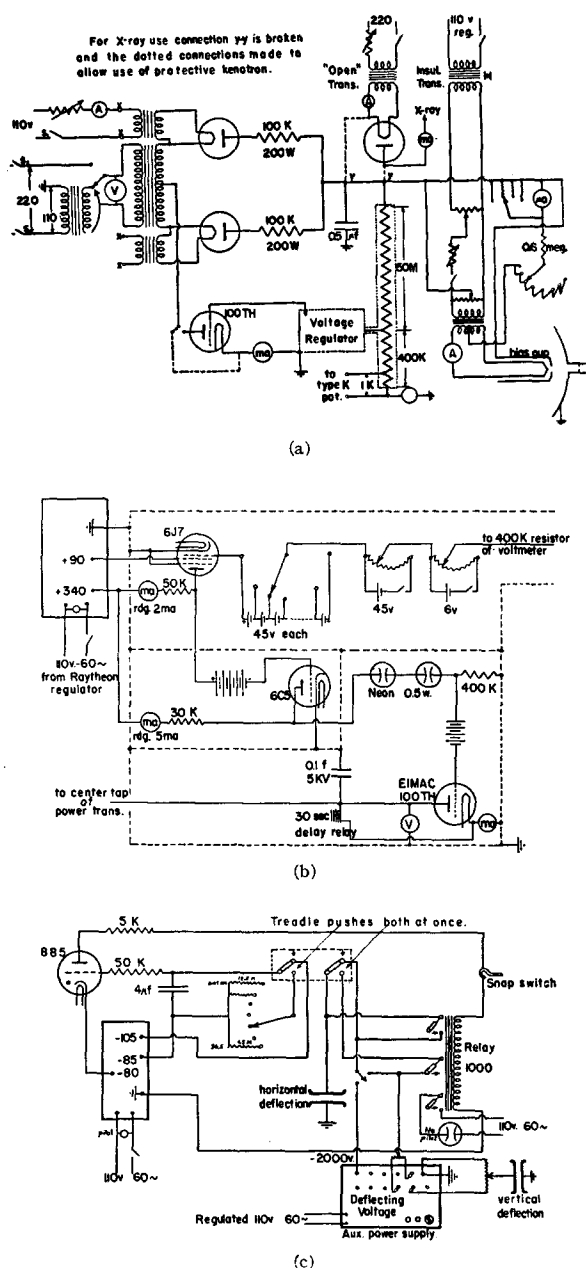
adjacent maxima to minima would result. The best smooth curve through these points is taken as the background.

(B) Average values are computed for the  $s$  positions at which the theoretical curves cross from positive to negative values, and vice versa. These are plotted on the microphotometer record and the best smooth curve drawn through them is taken as the background. Experience has shown that the background curves are not sensitive to the selection of models used in the averaging processes when these nearly represent the correct structure, and that the backgrounds deduced by means of procedures (A) and (B) differ very little from each other. Models which depart appreciably from the correct structure will lead to points which scatter badly from a smooth curve. Then, as a first approximation, the intensity of the molecular term relative to the atomic terms (taken as unity) is the ratio of the density indicated by the microphotometer trace to that of the background at each value of  $s$ . This is valid only when extraneous scattering and other factors which disturb the theoretical relation (3) between the atomic and molecular terms, are negligible in magnitude.

## THE PHOTOGRAPHS

Electron diffraction pictures of neopentyl, and silico-neopentyl chlorides were taken on samples generously given to us by the late Dean F. C. Whitmore. Pictures with and without a sector were taken of both compounds. Three sectors were used for the neopentyl chloride covering the range from  $s=0$  to  $s=9$ , 14, and 20, respectively, while two sectors were used for the silico-neopentyl chloride going out to  $s=11$ , and 16.5, respectively. A visual estimate of the  $I(s)$  curve based on pictures taken with and without a sector for the neopentyl chloride is shown in Fig. 11, curve A, while that for the silico-neopentyl chloride is curve C. The points of inflection of the visual  $I(s)$  curves were obtained by direct measurement on a comparator; the hairline being set in each case on the point of apparent maximum or minimum density. The amplitudes of these visual  $I(s)$  curves were determined by drawing in a background and arbitrarily setting the most intense peak equal to ten and the least intense equal to a half-unit, above this background. The intermediate region was then estimated on this scale. Curves B and D are the result of microphotometer measurements on sector pictures of neopentyl chloride and silico-neopentyl chloride, respectively. The positions of the maxima and minima for these curves were determined by drawing in a background (as indicated in the previous section), and choosing those points which showed the largest difference from this background.

The  $s_0$  values of the maxima and minima for the visual curves are given in Tables I and II, while those for the sector curves are indicated in Fig. 11. The self-consistency among the individual visually estimated  $s_0$



values is such that the probable error is of the order of a half of one percent. In the case of the sector curves, the  $s_0$  values were measured to a tenth of an  $s$  unit and to this accuracy no deviations were observed among six different microphotometer records. In the case of the neopentyl chloride the sector curve could not be extended beyond  $s=14$ , even though a sector was cut for  $s=20$ , because the intensity was so low; at the last observed maximum ( $s \approx 12.5$ ) the intensity at the peak was only four percent above the background. The amplitudes of the sector  $I(s)$  curves are in doubt in the region  $s \leq 4$

because of the extraneous background introduced by the undeiated beam and by multiple scattering.

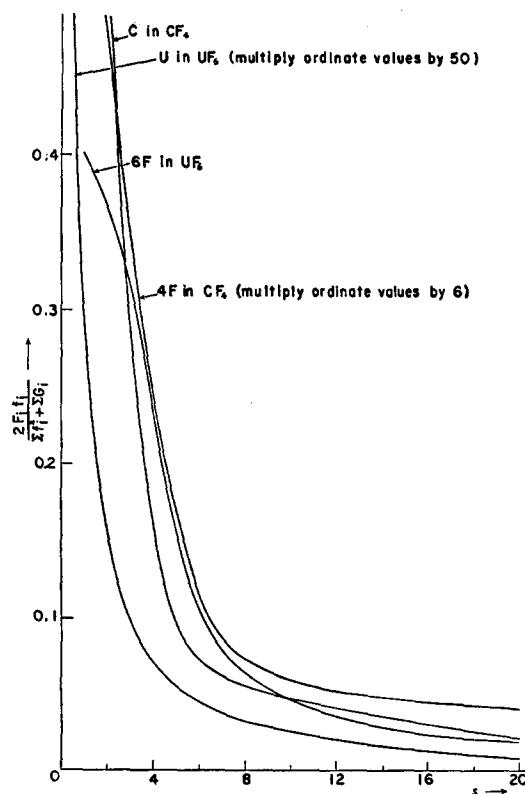
A comparison of the visual and sector  $I(s)$  curves shows a very good check in the case of the silicone-pentyl chloride. For the neopentyl chloride, however, there is an appreciable difference between the two curves from  $s > 8$ . This difference will be discussed in more detail when a comparison between theoretical and observed  $I(s)$  curves is made.

## INTERPRETATION OF THE DATA

### Radial Distribution Curves

Radial distribution curves computed from the visual  $I(s)$  curves are shown in Fig. 12 together with "synthetic" distribution plots. The method used was that of Walter and Beach.<sup>11</sup> The synthetic radial distribution curves are semi-empirical in nature since they are based on an average form of the peaks (arbitrarily terminated for  $|r-r_{ij}|=0.325\text{\AA}$ ) for the several different molecules examined by Walter and Beach. A constant shape has been assumed for all distances between directly and adjacently bonded atoms; the standard curve was then multiplied by the weight factor  $Z_i Z_j$ .

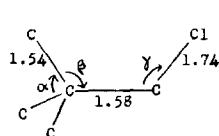
For the neopentyl chloride we have been able to match the synthetic curve B to the calculated one A



<sup>11</sup> J. Walter and J. Y. Beach, J. Chem. Phys. 8, 601 (1940).



rather well except for the peak at  $r=1.57\text{\AA}$  using the model:



$$\begin{aligned}\alpha &= 108^\circ \\ \beta &= 111^\circ \\ \gamma &= 111^\circ \\ \text{C-H} &= 1.09\text{\AA} \\ \angle \text{HCH} &= 109.5^\circ.\end{aligned}$$

The discrepancy at  $r=1.57$  might be avoided by lengthening all the C-C bonds, but then other difficulties are introduced. Another possibility would be to widen somewhat the "synthetic" peak shapes. If one assumes the normal C-C distance of 1.54 and C-Cl 1.76, the discrepancy becomes more marked as can be seen from Fig. 12, curve C. The sharpness of the peaks at 3.19 and 4.13 which result from



respectively, indicates that the barrier height restricting rotation about the  $\text{C}_1\text{--}\text{C}_2$  bond is relatively large compared to  $kT$ . Hence these  $\text{C} \longleftrightarrow \text{Cl}$  contribu-



tions to the scattering curve can be approximated by constant  $r_{\text{C-Cl}}$  values in the  $\sin sr_{\text{C-Cl}}/sr_{\text{C-Cl}}$  terms; to

allow for the limited oscillation the corresponding temperature factors were increased.

Calculated D and synthetic E curves for silico-neopentyl chloride are also given in Fig. 12. The match between the two is not as good as in the previous case. The model which gives the best agreement has

Si-C	1.88\AA
C-Cl	1.73\AA
C-H	1.09\AA

all angles tetrahedral.

A distortion similar to the one used for neopentyl chloride is not satisfactory. The calculated curve does

not show prominent Si-C distance whereas the synthetic curve indicates a strong maximum at this point. This lack of resolution may be due to the influence

of the very large Si-C contribution. The match for  $r > 3$  is necessarily poor due to the method of constructing the "synthetic" curve, since no direct allowance was made for rotation about the Si-C bond, which becomes appreciable for these longer distances. This clearly indicates that the barrier to rotation is lower in the case of the silicon compound than the corresponding carbon one, as is to be expected.<sup>12</sup>

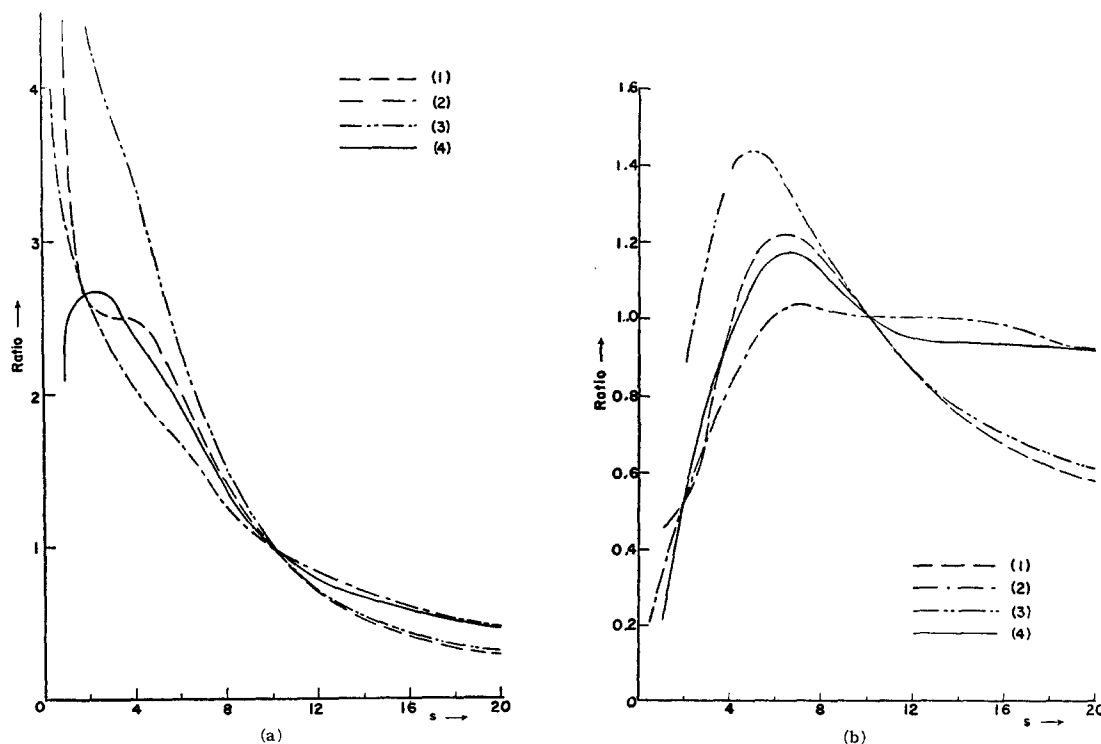
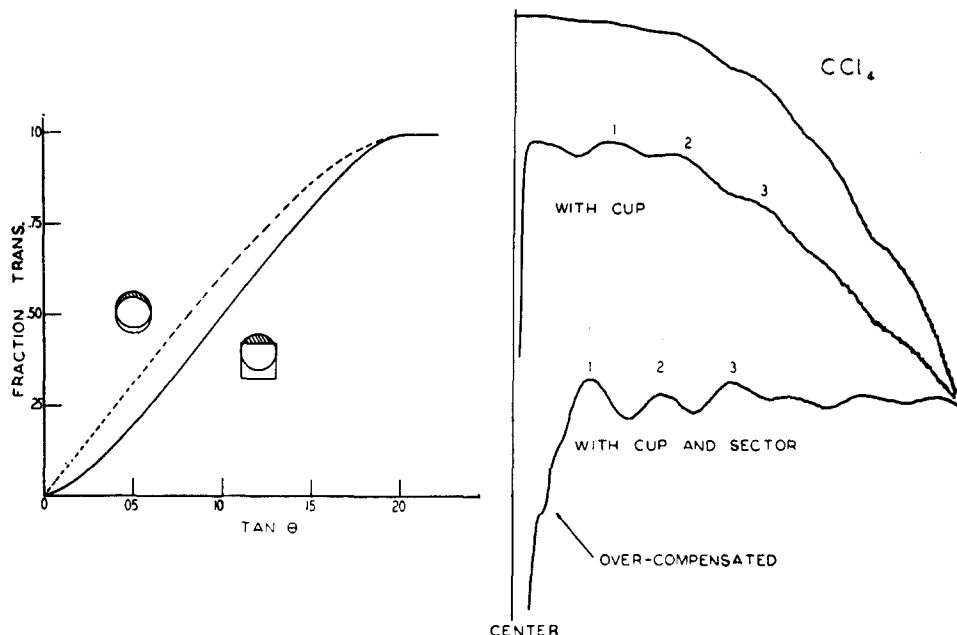


FIG. 8. Backgrounds expected for various compounds when (a)  $s^2$  sectors and (b)  $s^3$  sectors are used. Ordinates are ratios of backgrounds expected to that computed with Eq. (2), for: (1)  $\text{CF}_4$ , (2)  $\text{UF}_6$ , (3)  $\text{H}_2\text{CO}$ , (4)  $\text{Cl}_4$ .

<sup>12</sup> Aston, Isserow, Szasz, and Kennedy, J. Chem. Phys. 12, 336 (1944).

FIG. 9. Left—the geometrical shadow, for an infinitesimal sample, cast by a square and by a round front beam stop. Right—typical unreduced microphotometer records for gas diffraction.



The largest error introduced in the radial distribution curve is due to the improper integration procedure used in the Fourier inversion. It is hoped that a better numerical integration based on the method of Lanczos-Danielson<sup>13</sup> or with an IBM punched card system<sup>14</sup> will be made. When this is carried through, the radial distribution curve will furnish valuable information about internal rotation.

### Correlation Method

In order to check the conclusions reached by fitting synthetic radial distribution curves to the radial distribution curves obtained from our intensity data, theoretical  $I(s)$  curves for several models for each compound were computed and compared with the patterns observed. In making these comparisons we found that the visual curves, A and C (Fig. 11), correspond fairly well to intensity patterns computed according to the simple expression

$$\sum_{ij} Z_i Z_j \frac{\sin sr_{ij}}{sr_{ij}} \exp(-a_{ij}^2 s^2), \quad (5)$$

where the  $a_{ij}$  is assumed to be zero for all but those pairs whose distances vary due to hindered rotation about single bonds. The microphotometer recordings (B and D of Fig. 11) show considerably less detail than is apparent to the eye. They should be compared to curves computed by means of Eq. (3). In the latter case, not only should one consider the general form of the curves, but also the measured intensities relative to the background

taken as unity. Since the maximum deviations from the background are only 12 percent, the structure sensitive features often are only of the order of one percent. But in attempting to realize an accuracy of one percent in the total density (which is equivalent to about eight percent of the molecular contribution at small  $s$ ), we are approaching the limit of photographic measurements due to grain size, inhomogeneities in the emulsion, and variations in development.

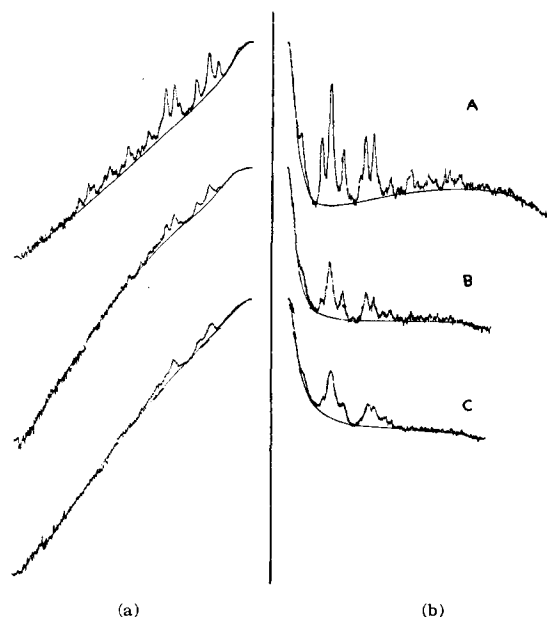


FIG. 10. Microphotometer records of electron diffraction patterns of powders, illustrating the usefulness of the sector as an aid in estimating diffraction line widths. (a) No sector. (b) Empirical sector. Spinels of decreasing size.

<sup>13</sup> Danielson and Lanczos, J. Frank. Inst. 33, 365, 435 (1942).

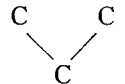
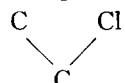
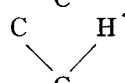
<sup>14</sup> Shaffer, Schomaker, and Pauling, J. Chem. Phys. 14, 659 (1946).

**Neopentyl Chloride (Fig. 13)**

We considered the following models:

All C—C=1.54Å  
C—H=1.09Å  
C—Cl=1.76Å  
all angles tetrahedral.

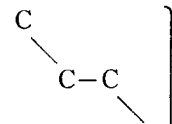
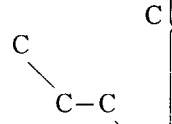
In curve A (Eq. (3) was used, wherein the integration over the distribution  $P(r_{ij})$  was given the usual  $\exp(-a_{ij}^2 s^2)$  form) we included all distances except the variable C—Cl and C—H, with the following temperature factors:

Atom Pair	$a_{ij}^2$	$\langle \Delta^2 \rangle_{Av} = (2a_{ij}^2)^{\frac{1}{2}}$
$\left. \begin{array}{c} \text{C—C} \\ \text{C—Cl} \\ \text{C—H} \end{array} \right\}$ 	0.0015	0.055Å
$\left. \begin{array}{c} \text{C—C} \\ \text{C—Cl} \end{array} \right\}$ 	0.0022	0.066Å
$\left. \begin{array}{c} \text{C—C} \\ \text{C—H} \end{array} \right\}$ 	0.0043	0.093Å

$\langle \Delta \rangle_{Av}$  is equal to the root mean displacement from the equilibrium separation of the particular atom pair, due to zero point energy.

In omitting the variable terms we have, in effect, assumed very large  $a_{ij}^2$  values for these distances.

B and B'. The same distances as in Model A plus a staggered configuration about the C—C bond were assumed, and the following additional temperature factors were used:

Atom Pair	$a_{ij}^2$	$\langle \Delta^2 \rangle_{Av} = (2a_{ij}^2)^{\frac{1}{2}}$
$\left. \begin{array}{c} \text{C} \\ \text{C—C} \\ \text{C} \end{array} \right\}$ 	B 0.0050 B' 0.0050	0.1Å 0.1Å
$\left. \begin{array}{c} \text{C} \\ \text{C—C} \\ \text{H} \end{array} \right\}$ 	B 0.0050 B' 0.0100	0.1Å 0.142Å

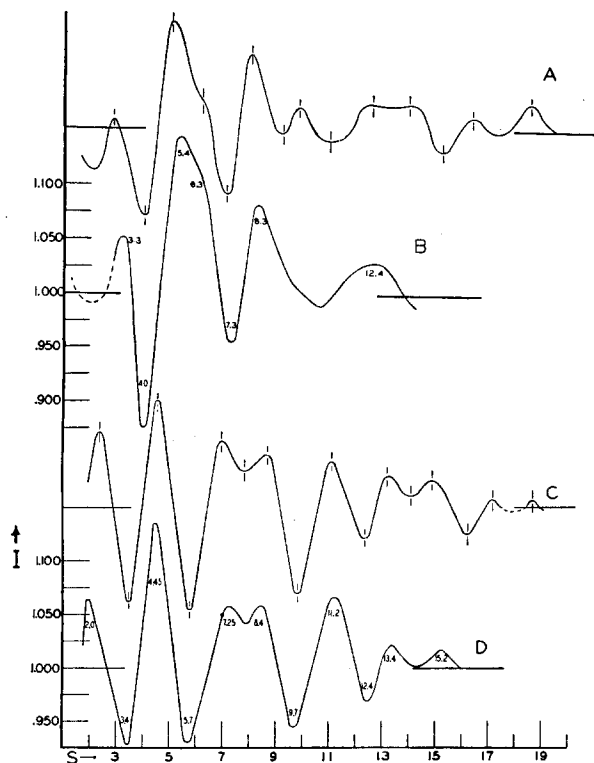
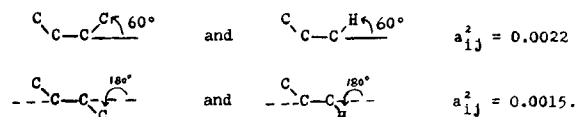


FIG. 11. Observed intensity patterns. A—visual estimates for  $(\text{CH}_3)_3\text{C—CH}_2\text{Cl}$ , B—microphotometer record  $(\text{CH}_3)_3\text{C—CH}_2\text{Cl}$ , C—visual estimate for  $(\text{CH}_3)_3\text{Si—CH}_2\text{Cl}$ , D—microphotometer record  $(\text{CH}_3)_3\text{Si—CH}_2\text{Cl}$ .

D and D'. In Models D and D' we assumed the distances and angles deduced from our radial distribution analysis. With regard to the temperature factors, D and D' correspond to B and B', respectively.

C. In Model C the distances and angles were again those derived from the radial distribution analysis computed, however, according to Eq. (5) with the  $a_{ij}^2 s = 0$  except for



Comparison of the curves in Figs. 11 and 13 shows that the structure sensitive regions are at  $s=6.3$  and in the intervals  $9 < s < 12$  and  $13.5 < s < 17.5$ . Curves A, B, B', and D show no distinct hump at  $s=6.3$ ; however, the peaks are definitely asymmetric and the magnitude of the hump as indicated may be exaggerated due to the difficulty of estimating a small fluctuation of intensity in a region of sharply falling intensity ( $5.2 < s < 7$ ). In curve C there is a strong suggestion of a hump at  $s=6.3$  which, if present in a photograph, would appear to the eye as a distinct shelf. The structure apparent visually in the region  $9 < s < 12$  is not properly reproduced by

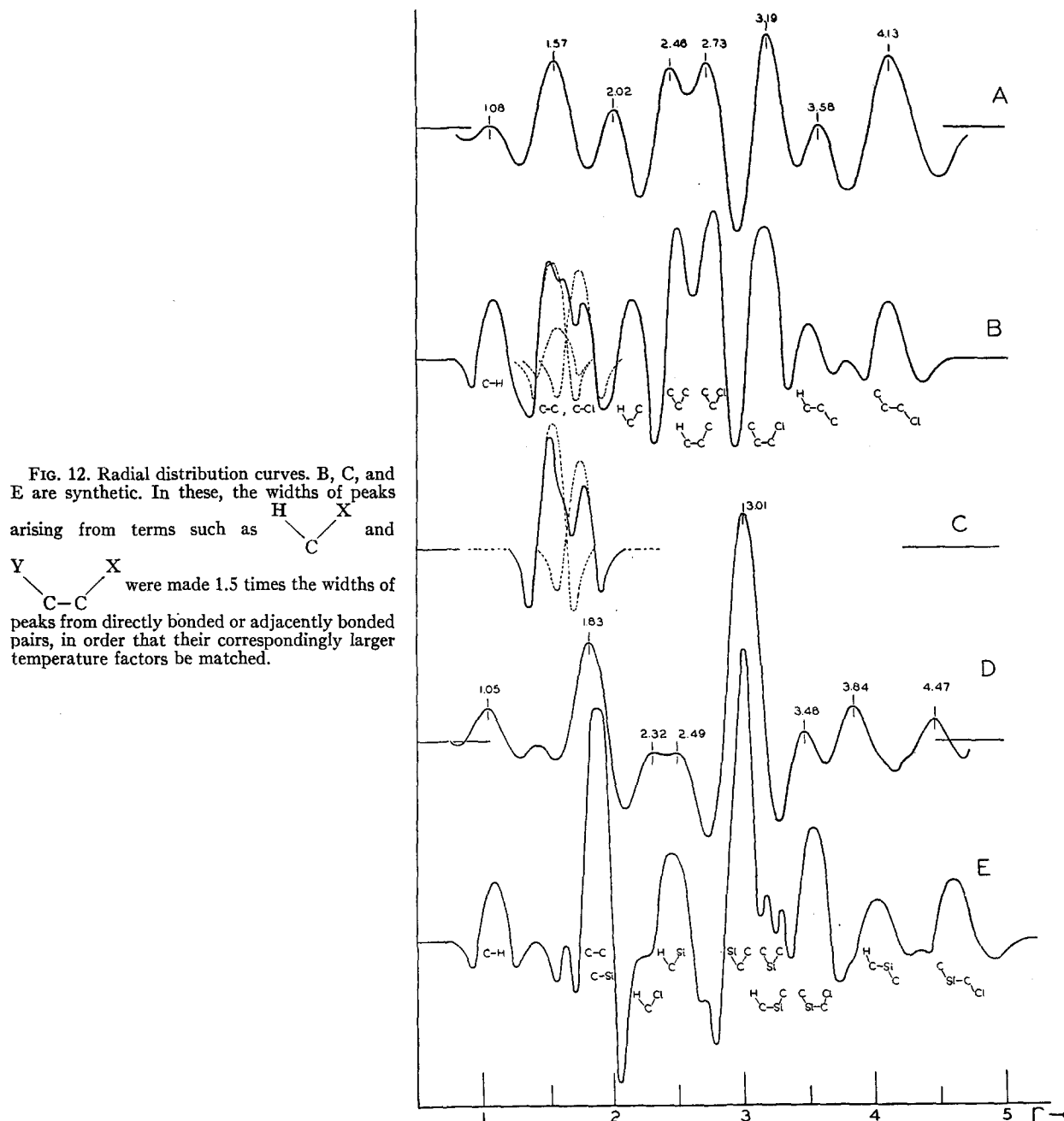


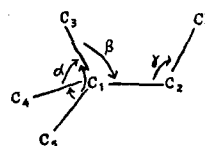
FIG. 12. Radial distribution curves. B, C, and E are synthetic. In these, the widths of peaks arising from terms such as  $\begin{array}{c} \text{H} \\ \diagup \\ \text{C} \\ \diagdown \\ \text{X} \end{array}$  and  $\begin{array}{c} \text{Y} \\ \diagup \\ \text{C}-\text{C} \\ \diagdown \\ \text{X} \end{array}$  were made 1.5 times the widths of peaks from directly bonded or adjacently bonded pairs, in order that their correspondingly larger temperature factors be matched.

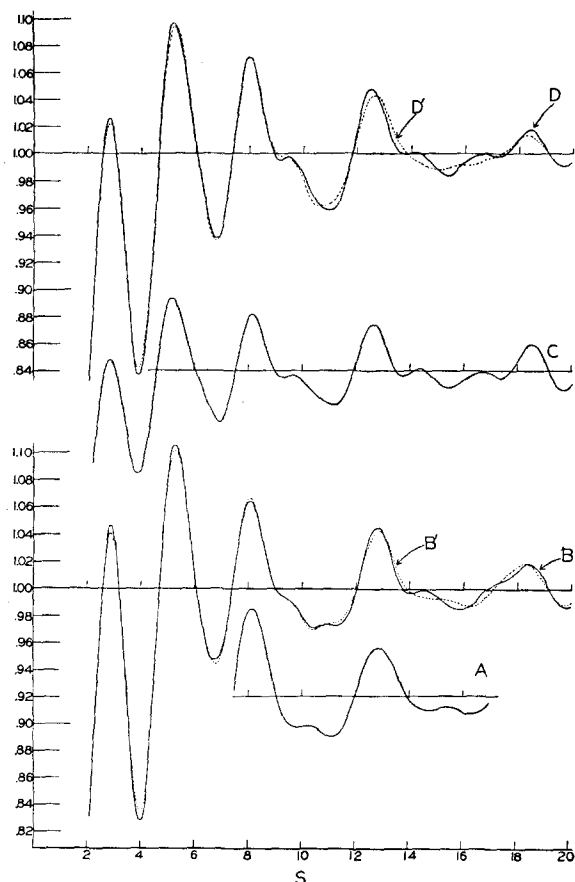
curves A, B, B', and D', but fairly well in C and D. The same is true in the region  $13.5 < s < 17.5$ .

Curve C is in best qualitative agreement with our visually observed  $I(s)$  curve. A curve computed in a manner similar to C, but with the distances and angles of model A (undistorted) is not acceptable. Furthermore, D and D' are more like our visually observed curve than are B and B'. Hence, we conclude that although the distortion is barely outside our experimental error it is probably real.

Unfortunately, our microphotometer record is not

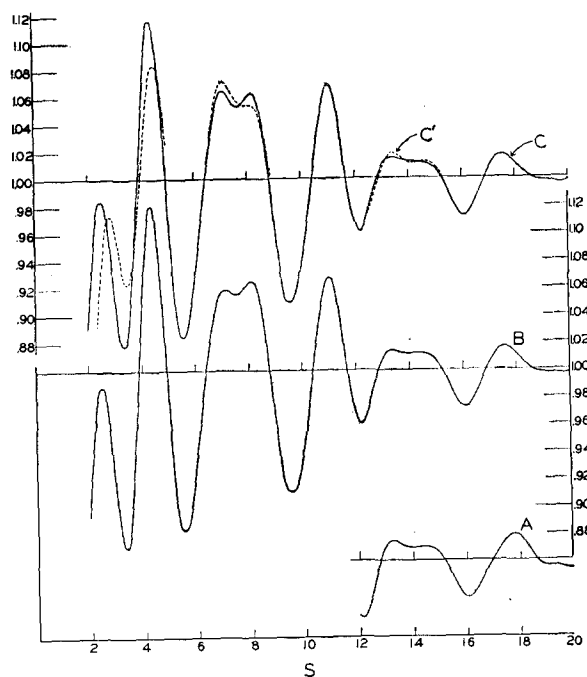
sufficiently detailed to permit a more definite selection of a model. The quantitative comparison of the experimental and theoretical  $I(s)$  curves is presented in Table I. Our best values for the interatomic distances and angles in neopentyl chloride are:



FIG. 13. Computed intensity curves for  $(\text{CH}_3)_3\text{C}-\text{CH}_2\text{Cl}$ .

All other

$$\begin{aligned} \text{C}-\text{Cl} &= 1.74\text{\AA} \pm 0.03 \\ \text{C}_1-\text{C}_2 &= 1.58\text{\AA} \pm 0.04 \\ \text{C}-\text{C} &= 1.54\text{\AA} \pm 0.03 \\ \text{C}-\text{H} &= 1.09\text{\AA} \text{ (assumed)} \end{aligned}$$

FIG. 14. Computed intensity curves for  $(\text{CH}_3)_3\text{Si}-\text{CH}_2\text{Cl}$ .

$$\begin{aligned} \angle \text{HCH} &= 109.5^\circ \text{ (assumed)} \\ \alpha &= 108^\circ \pm 2^\circ \\ \beta &= 111^\circ \pm 2^\circ \\ \gamma &= 111^\circ \pm 2^\circ \end{aligned}$$

**Silico-Neopentyl Chloride (Fig. 14)**

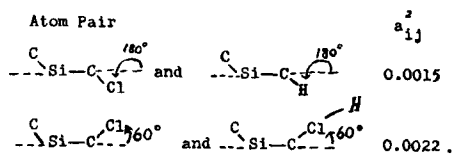
The following models were considered:

$$\begin{aligned} \text{A.} \quad & \text{C}-\text{Si} = 1.88\text{\AA} \\ & \text{C}-\text{Cl} = 1.73\text{\AA} \\ & \text{C}-\text{H} = 1.09\text{\AA} \\ & \text{all angles tetrahedral.} \end{aligned}$$

TABLE I. Neopentyl chloride.

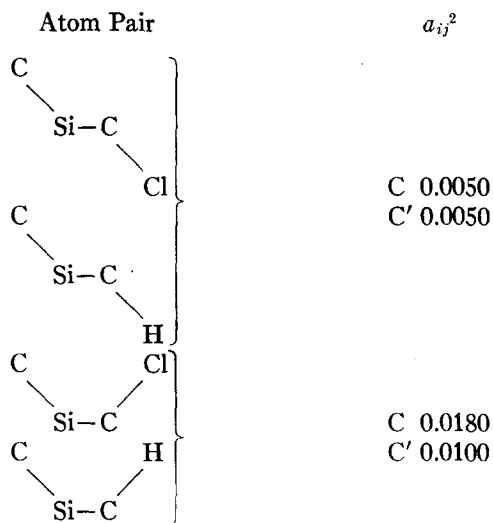
Max.	Min.	$s_0$ (vis.)	$I$ (vis.)	$\frac{s_0 \text{ comp.}}{s_0 \text{ obs.}} (\text{C})$	$\frac{s_0 \text{ comp.}}{s_0 \text{ obs.}} (\text{D})$	$I_{\text{comp}} (\text{D})$	$I_{\text{mpr}} (\text{D})$	$\frac{I_{\text{comp}}}{I_{\text{mpr}}}$
1		2.86	+1	0.983	0.986	1.027	(1.107)	
	2	4.04	-8	(0.948)	0.965	0.838	0.875	0.957
2		5.06	+10	1.008	1.029	1.097	1.142	0.960
2a		6.02	+3	1.023				
	3	7.11	-6	0.968	0.959	0.938	0.955	0.982
3		8.02	+7	1.006	0.998	1.072	1.080	0.992
	4	8.91	-1	0.979	1.028	0.995	0.953	1.044
4		9.80	+2	0.979	0.961	0.997		
	5	11.39	-3.5	0.975	0.964			
5		12.62	+4	0.994	0.990	0.958		
	6	13.23		1.034	1.043	1.047	1.045	1.001
6		13.93	+3.5	1.027	1.020			
	7	15.21	-2	1.012	1.009			
7		16.30	+3	1.023	1.030			
	8							
8		18.56	+1	0.992	0.994			
Average = 1.000					0.998			
Mean deviation = 0.018					0.024			

This model corresponds to the one deduced from the radial distribution curve. It was computed using Eq. (5), assuming  $a_{ij}^2=0$  for all pairs except for those distances which vary due to rotation. The temperature factors used for the latter were:



B. The same distances and angles were assumed as in model A, but Eq. (3) was used. The varying C-Cl and C-H distances were omitted. The  $a_{ij}^2$ 's used for curve B were the same as those used for the carbon compound.

C and C'. This model is identical with B, including a staggered configuration about the C-Si bond. The additional temperature factors were:



The regions of comparison for this substance are  $6.5 < s < 8.5$  and  $13 < s < 15$ . The visual and microphotometer curves (C and D of Fig. 11) are in complete agreement. In the region  $6.5 < s < 8.5$ , A is very similar to model B which reproduces the relative intensities of the visually observed doublet. Model C, having a larger temperature factor for the varying pairs than does C', is in closer agreement with the relative intensities of the doublet as deduced from the microphotometer record. Neither of the models reproduces exactly the relative intensities of the doublet occurring in the region  $13 < s < 15$ . The fluctuation above or below the background, however, is not more than one percent so that the doublet in curves C and D of Fig. 11 may actually not be as prominent as drawn.

Curve C (Fig. 14) is in best agreement with the microphotometer record; the large temperature factors used indicate a relatively low barrier hindering rotation about the C-Si bond as compared with the barrier in neopentyl chloride. This checks the conclusions reached from the radial distribution method. The quantitative comparison is given in Table II. The best values for the interatomic distances and angles in silico-neopentyl chloride are:

$$\begin{aligned} \text{C-Si} &= 1.88\text{\AA} \pm 0.04 \\ \text{C-Cl} &= 1.73\text{\AA} \pm 0.03 \\ \text{C-H} &= 1.09\text{\AA} \pm (\text{assumed}) \\ \text{all angles} &= 109.5^\circ \pm 2^\circ. \end{aligned}$$

## DISCUSSION OF RESULTS

### Visual and Sector Methods

Firstly, the introduction of a stop just past the point of diffraction has several advantages. It helps clear up the inner portion of the photograph so that the  $s_0$  values for this region may be obtained more easily. At the same time it enables one to make more reliable intensity estimates of the inner portion of the diffraction pattern. The introduction of a beam stop would probably require

TABLE II. Silico-neopentyl chloride.

Max.	Min.	$s_0$ (vis.)	$I$ (vis.)	$\frac{s_0 \text{ comp.}}{s_0 \text{ obs.}} (\text{C})$	$I_{\text{comp}}(\text{C})$	$I_{\text{mpr}}(\text{C})$	$\frac{I_{\text{comp}}}{I_{\text{mpr}}}$
1		2.38	+7	1.046	0.984		
		3.47	-9	0.962	0.878		
2	2	4.54	+10	0.966	1.117	0.927	0.947
	3	5.87	-10	0.952	0.884	1.135	0.984
3		6.95	+6	1.021	1.064	0.930	0.950
	4	7.81	$-\frac{1}{2}$	0.983	1.054	1.057	1.006
4		8.68	+5	0.943	1.063	1.043	1.010
	5	9.81	-8	0.977	0.910	1.058	1.004
5		11.09	+5	0.994	1.068	0.945	0.962
	6	12.33	-3	0.991	0.961	1.066	1.002
6		13.15	+3	1.020	1.015	0.970	0.990
	7	14.06	$-\frac{1}{2}$	1.001	1.012	1.021	0.994
7		14.86	+2.5	0.985	1.011	0.988	1.024
	8	16.21	-3	0.993		1.017	0.994
8		17.14	$+\frac{1}{2}$	1.022			
Average=0.990							
Mean deviation=0.022							

very little redesigning of most existing cameras. However, a serious objection against the use of a beam trap along with a sector is the difficulty of properly allowing for the shadow function in cutting the sector. Another undesirable feature is the extraneous edge scattering when the width of the stop is just a little greater than that of the primary beam.

Secondly, the sector technique is the only reliable method which can be used to obtain intensity data with photographic detection. Its inherent accuracy is limited by the fact that the total electron scattering is recorded, whereas structure determinations depend on the molecular term only. For this reason, the sector method will not displace the visual method for structure determinations; however, it will be of invaluable aid in deciding between parameters on the basis of, which member of a doublet is the more intense, the height and presence of shoulders, etc. It will also be useful for estimating the magnitude of large temperature factors. Use of the sector does provide a means for calibrating the visual method.

With sector data there are three checks on the maximum variation of the parameters which can be allowed. They include the two employed in the visual method; *viz.*, the matching of the synthetic radial distribution curves with the one obtained from the data, and the matching of over-all shape (relative peak heights) as well as the  $s_0$  values of the theoretical  $I(s)$  curve with these observed. In addition, one may compare point by point the observed intensity with that of the theoretical  $I(s)$  curve.

Reference to the last column of Tables I and II shows that for values of  $s > 7$  the computed intensities check very well with the measured ones. In the region  $s < 7$ , the drawing-in of the background cannot be performed in a satisfactory manner. Such disturbing effects as arise from finite sample and beam dimensions, multiple scattering and the lack of good atom form factor values are largest for low  $s$  values. With regard to the determination of reliable coherent and incoherent atom form factors, a study of a series of diatomic and simple polyatomic molecules is contemplated.

#### Regarding $(\text{CH}_3)_3\text{C}-\text{CH}_2\text{Cl}$ and $(\text{CH}_3)_3\text{Si}-\text{CH}_2\text{Cl}$

The two molecules studied permit an assessment of the applicability of electron diffraction technic to the study of internal rotation. For the neopentyl chloride, a very satisfactory fit was obtained between computed and synthetic radial distribution curves. Models without distortion, or those in which normal covalent distances (all C—C 1.54; C—Cl 1.76) were assumed, could not be made to fit. The radial distribution analysis also indicated that the configuration was a staggered one with relatively little motion about the C—C bonds. The correlation procedure confirmed these conclusions rather well. For the silico-neopentyl chloride the radial distribution curve indicated a staggered configuration with a low barrier to rotation about the C—Si bond, as well

as a shortening of the C—Cl distance. The correlation method confirmed these conclusions also. The intensity data were valuable in determining the magnitude of the temperature coefficient in the silicon compound. However, the present intensity data for the neopentyl chloride are not sufficiently detailed to enable one to make a clear-cut choice of temperature factors.

One may present plausible interpretations for the deviation of the distances and bond angles in these compounds from the values which are currently considered "normal." He may argue that two effects, both operating in the same directions, introduce distortions in neopentyl chloride. (a) The  $-\text{CH}_2\text{Cl}$  group is sterically larger than the  $-\text{CH}_3$  group; (b) the  $-\text{CH}_2\text{Cl}$  group is electron seeking ( $-I$ ) compared to the  $-\text{CH}_3$  group. This tends to draw electron density toward the  $\text{Me}_3\text{C}-\text{CH}_2\text{Cl}$  bond, making it relatively more  $p$  and less  $s$  in character compared to hybridized, truly tetrahedral  $sp^3$ . As a result, the  $\text{Me}_3\text{C}-\text{CH}_2\text{Cl}$  bond is longer ( $1.58 \pm 0.04\text{\AA}$ ) than the  $\text{Me}_3\text{C}-\text{CH}_3$  bond ( $1.54 \pm 0.02\text{\AA}$ ).<sup>15</sup> Further, the  $\angle \text{C}_1\text{C}_1\text{C}_2$  angle is smaller ( $108 \pm 2^\circ$ ) than the corresponding angle in *t*-butyl chloride ( $111.5 \pm 2^\circ$ );<sup>16</sup> it is rather, more like the nitrogen valence angle in trimethyl amine ( $108 \pm 4^\circ$ ).<sup>17</sup> It is doubtful whether the small apparent departure of the C—Cl distance from the sum of radii<sup>18</sup> (1.76\AA) or from that found in  $\text{Me}_3\text{C}-\text{Cl}$  ( $1.78 \pm 0.03\text{\AA}$ ) is significant.

In the silico-neopentyl chloride no distortion about the silicon atom is observed; the average Si—C distance is equal to the sum of radii<sup>18</sup> ( $1.88 \pm 0.4\text{\AA}$ ), and to that found in hexamethylcyclotrisiloxane ( $1.88 \pm 0.04$ ).<sup>19</sup> The value reported for silicon tetramethyl is somewhat larger ( $1.93 \pm 0.03$ ).<sup>17</sup> In this case, due to the larger Si— $\text{CH}_2\text{Cl}$  distance, the steric effect does not come into play, nor is the ( $-I$ ) factor significant, since the Si—C bond has considerably more ionic character than the C—C bond. However, the  $\text{Me}_3\text{SiCH}_2-\text{Cl}$  is somewhat shorter ( $1.73 \pm 0.03\text{\AA}$ ) than the C—Cl distance in *t*-butyl chloride.<sup>16</sup> Perhaps it is a consequence of the greater electron-seeking character of  $\text{Me}_3\text{SiCH}_2-$  compared to  $\text{Me}_3\text{C}-$  and  $\text{Me}_3\text{CCH}_2-$ ; this would tend to increase the  $s$  character of the C—Cl bond, and make it shorter.

#### ACKNOWLEDGMENTS

We wish to acknowledge the kindness of the late Dean F. C. Whitmore who furnished highly purified samples of the neopentyl chloride and silico-neopentyl chloride. We also wish to express our sincere thanks to Mr. H. S. Bush for his patience and cooperation in the construction of the apparatus.

<sup>15</sup> L. Pauling and L. O. Brockway, *J. Am. Chem. Soc.* **59**, 1223 (1937). F. Rogowski, *Ber. Deut. Chem. Gesel.* **72**, 2021 (1939).

<sup>16</sup> J. Y. Beach and D. P. Stevenson, *J. Am. Chem. Soc.* **60**, 475 (1938).

<sup>17</sup> L. O. Brockway and H. O. Jenkins, *J. Am. Chem. Soc.* **58**, 2036 (1936).

<sup>18</sup> V. Schomaker and D. P. Stevenson, *J. Am. Chem. Soc.* **63**, 37 (1941).

<sup>19</sup> Eleanor (Weller) Aggarwal and S. H. Bauer (unpublished).

<sup>20</sup> F. C. Whitmore and L. H. Sommers, *J. Am. Chem. Soc.* **68**, 481 (1946).